AIAA JOURNAL
Vol. 48, No. 9, September 2010

Computational Simulations of the Effect of Backstep Height on Nonpremixed Combustion Instability

R. Smith,* G. Xia,† W. A. Anderson,‡ and C. L. Merkle§
Purdue University, West Lafayette, Indiana 47907

DOI: 10.2514/1.40385

Detailed computational simulations are used to compare the effect of backstep height on the stability characteristics of an axisymmetric dump combustor fed by separate fuel and oxidizer streams. Companion experiments demonstrate a dramatic increase in the amplitude of pressure oscillations for the smaller backstep due to combustion instability. The goal of the present simulations is to ascertain whether computations can predict combustion instability for this configuration and the degree to which they can replicate this experimental trend. Two different oxidizer-inlet boundary conditions were used: a subsonic inlet and a choked inlet. Both predicted stronger oscillations for the smaller backstep, although the disturbances in the uniform inlet case decayed to relatively low levels. The oscillations in the choked-inlet case were sustained but were still somewhat smaller than in the experiment. The simulations suggest the effect of backstep height arises because of stronger wall/vortex impingement in the smaller-step-height combustor. The instantaneous pressure and heat release are more strongly in phase for the smaller-step-height simulations, resulting in larger Rayleigh indices. Power spectral density results likewise show larger peaks for the smaller step. The sensitivity to upstream conditions suggests that care should be taken in designing both simulations and experiments.

I. Introduction

INSTABILITY often occurs in combustors when the dynamic heat release from combustion couples with the natural acoustic modes of the geometry. This coupling causes growth of pressure perturbations that can potentially develop into large amplitude fluctuations. Such fluctuations can introduce large thermal and mechanical stresses in the combustor, resulting in decreased performance, unacceptable vibrations or even engine failure. Our focus in the present paper is on instability in high-pressure choked combustors with nonpremixed fuel and oxidizer streams such as those employed in rocket engines. In such applications the energy release rates are very high and combustor volumes are often nearly acoustically closed, such that small perturbations can grow to destructive amplitudes very quickly. This potential for strong coupling has made combustor design more difficult and expensive for liquid rocket engines because of the uncertainty and extensive testing required to verify stable combustion [1–5]. Precautionary elements such as resonant cavities and baffles are often added to the design in an effort to avoid instabilities.

Various levels of modeling have been employed to deal with combustion instability. Engineering level models based upon wave equations and transfer functions representing the boundary conditions and unsteady heat release have proven the most popular for predicting relative growth rates of acoustic modes [6–9]. Such approaches allow for rapid parametric studies but have limitations in incorporating the complexities of both physics and geometry. In particular, such analyses must incorporate the all-important unsteady heat release by means of a phenomenological model. Computational fluid dynamics (CFD) procedures promise capability for more detailed analyses in which the unsteady heat release is computed as a part of the solution. The most detailed (and presumably the most desirable) level of CFD analyses is direct Navier-Stokes solutions, but CPU requirements for direct numerical simulation for combustion instability are far beyond the realm of practicality and will continue to be so for the foreseeable future. Large-eddy simulations (LES) represent the next logical subset of CFD analyses and, while still requiring large amounts of resources in conjunction with carefully designed subgrid models, they are starting to be applied to instability applications in some fields [10–12]. Less computationally intensive CFD analyses can be obtained by using the unsteady Reynolds-averaged Navier–Stokes (RANS) equations for modeling turbulence, but here more of the unsteady heat release must be modeled. Other modeling approaches that lie between the CFD and engineering level models also exist in which the acoustics of the system and the dynamic heat release are taken into account in different manners [8,9,13–18]. Nevertheless, even with the highest levels of modeling, validation against experimental data is still necessary to ensure that the instability of the system is accurately characterized.

Detailed computational analyses of the instability characteristics of solid rocket engines and ramjet combustors have been available for a number of years but are relatively new in gas turbine combustors and liquid rocket engines. Combustion instability in solid rockets is routinely modeled by RANS-based computational approaches that are generally accepted as being predictive, although the unsteady heat release from the burning solid must be empirically modeled for each propellant formulation. Analyses of premixed dump combustors representative of those used in ramjets were first reported by Menon and Jou [11], who used a two-dimensional version of an LES formulation. Although these early computations were forced to use relatively coarse grids, they were able to predict disturbance growth.

Initial applications of LES predictions in gas turbine combustors are just being reported. Martin et al.'s [12] recent simulations focus on the distinction between reflective and nonreflective downstream boundary conditions and the manner in which they lead to disturbance growth. Huang et al. [19] have reported a pioneering look at flame dynamics in gas turbine combustors as modeled by computational methods. Relatively early CFD simulations [17,20] of liquid rocket engine instability focused on pertinent formulations and global behavior, but did not predict unsteady heat release and were limited in grid resolution. More recent analyses have used LES methods to investigate short-duration predictions of forced oscillations in a rectangular combustor [21]. Detailed LES and

Presented as Paper 2008-5250 at the 44th AIAA/ASME/SAE/ASEE Joint Propulsion Conference and Exhibit, Hartford, CT, 21–23 July 2008; received 12 August 2008; revision received 23 December 2008; accepted for publication 9 January 2009.

*Graduate Research Assistant. Student Member AIAA.
†Senior Research Scientist. Member AIAA.
‡Professor. Member AIAA.
§Vincent P. Riley Professor of Engineering. Member AIAA.

RANS analyses of the unsteady dynamics in model rocket combustors have recently been reported by Tucker et al. [22], whose focus was on predicting time-averaged wall heat flux measurements rather than combustion instability.

Instability in liquid rockets is still poorly understood, with considerable argument as to the mechanisms that lead to disturbance growth and/or sustained oscillations. One of the most challenging issues confronting early analyses of rocket engine combustion instability was finding a mechanism that would drive instability [1]. Mechanistic analytical models require an appropriate lag between the heat release and the acoustic environment to realize growth and the first models predicted absolute stability. Chemical-reaction times were too rapid to generate instability and mixing modeled in a time-averaged sense failed to give an appropriate phase lag. Eventually, it was shown that the time lag that included internal heating of liquid droplets was sufficient to provide growth in an analytical model, but again, the unsteady heat release had to be incorporated by mechanistic models.

Computational simulations, in principle, provide the ability to model at least the larger scales of unsteady mixing and the ensuing unsteady heat release. However, there is no assurance that such analyses will provide disturbance growth. A challenging issue with any computational analysis is that even unstable combustors have regions of stability (depending on parameters such as the pressure level, oxidizer-to-fuel ratio and propellant characteristics) and some guidelines must be available for identifying regions of stability and instability. In the present paper, we use recent experimental measurements in a model rocket combustor [13,23–25] to distinguish stable and unstable regimes and use computational techniques to ascertain if similar trends can be observed.

The goal of the present paper is to use detailed computational analyses to simulate both the unsteady heat release and the resulting combustion dynamics in a model rocket engine and to compare the predicted trends with recently reported experimental measurements [23–26]. A question of specific importance is whether the unsteady heat release can be simulated in a manner that is sufficiently realistic to allow self-sustained oscillations. This question is addressed by adopting a formulation that tracks the large-scale mixing dynamics directly, and subgrid-scale events and boundary-layer details are modeled by means of an unsteady RANS model in an approach that is philosophically analogous to detached-eddy simulation (DES) [27]. The method differs from DES analyses in that a two-dimensional (axisymmetric) formulation is used. This appears to be the simplest analysis that has capability for direct prediction of the unsteady heat release. The two-dimensional formulation allows much finer grid resolution than is practical with a three-dimensional representation and enables much longer simulation times while still allowing important parametric studies of the nature needed to understand trends. The present computations have employed grids of nominally 350,000 cells (similar resolution in three dimensions would be approximately 250 million cells) and have been run out to 100 ms, with approximately 10 simulations being conducted. This grid resolution, temporal duration, and number of simulations are not practical for three-dimensional computations on current computers.

Finally, it is also useful to document the global characteristics that can be expected from two-dimensional simulations and their utility as a diagnostic tool. The dominance of boundary layers and wall effects in the near-injector mixing and flame-holding regions [22] favors DES over LES models which are more difficult to implement in near-wall regions.

The model liquid rocket combustor experiments that are mimicked in the present simulations introduce the oxidizer through a cylindrical channel, with the fuel being introduced in a concentric annulus. The configuration features a sudden expansion just downstream of the fuel injection location, a configuration somewhat analogous to the ramjet configuration cited previously [11], except that the ramjet operates in premixed mode, whereas the rocket involves nonpremixed combustion at much higher pressures. The experiments have shown that a 30% reduction in the backstep height of this sudden expansion leads to over an order of magnitude increase in oscillation amplitudes. The present analyses mimic the geometry and flow conditions of these experiments, with a view to discerning whether computational simulations can replicate these observed experimental trends. To the authors' knowledge, this represents the first reported attempt at using CFD simulations to predict observed instability trends in a model liquid rocket combustor.

The paper is structured in the following manner. First, a synopsis of the experimental configuration and the resulting unsteady pressure response is given. Next, the computational model is described briefly. The final section presents the results of a number of cases and compares predictions for the two chamber step heights. A special feature of these comparisons is an assessment of different types of upstream boundary conditions and the manner in which the upstream disturbances they introduce impacts downstream disturbance growth.

II. Experimental Configuration and Computational Model Formulation

A. Experimental Configuration

The specific geometry considered is modeled after experimental tests performed by Miller et al. [23,24] and Sisco [25] to study longitudinal combustion instability in a choked, high-pressure combustion chamber. In the experiments, the fuel and oxidizer were introduced into the combustion chamber by means of a coaxial injector configuration followed by a backstep into a dump combustor. The oxidizer was decomposed hydrogen peroxide (H_2O_2), and JP-8 was used as the fuel. A generic schematic of the experimental configuration is given in Fig. 1 along with a close-up view of the oxidizer and fuel manifolds in Fig. 2. The oxidizer was injected radially into the central oxidizer post through holes near its midpoint, and the fuel was injected tangentially with swirl through an annulus just ahead of the combustor. Note that the far left end of the oxidizer post was closed in an attempt to provide the most reflective upstream condition for promoting instability. To choke the exhaust flow and control the chamber pressure, a short converging nozzle was placed at the end of the combustor.

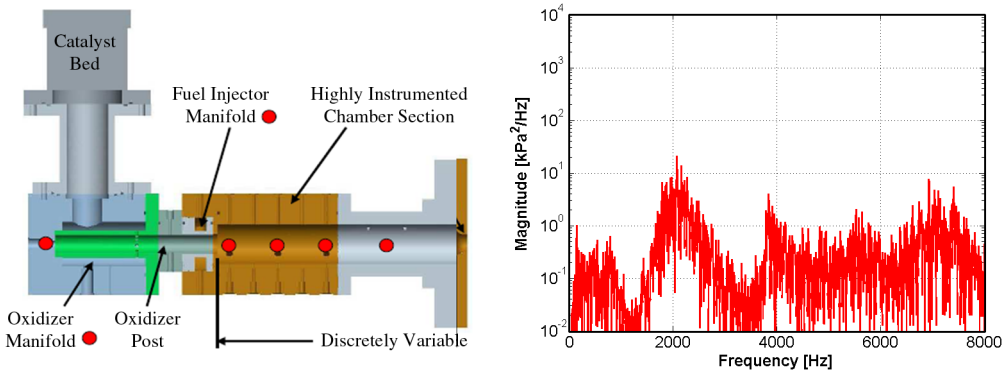

Fig. 1 Configuration of the original 25.4 cm (10 in.) combustor experiment (left) and PSD plot showing a classically stable response (right) [24].

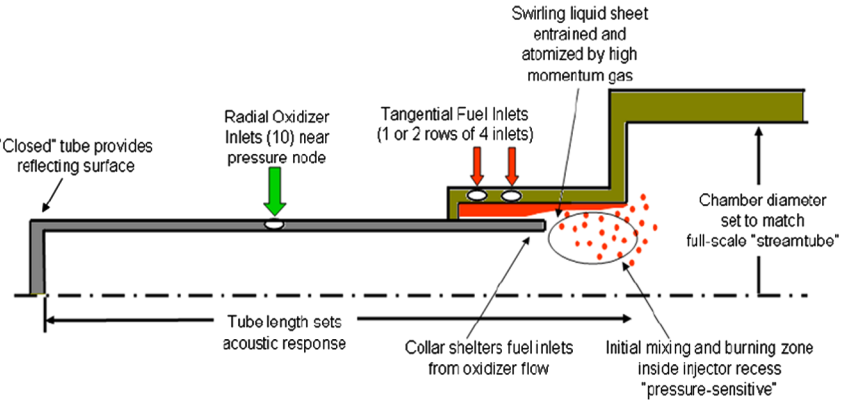

Fig. 2 Close-up schematic of the experimental injector configuration [24].

The first set of experiments [23] included tests of a series of combustor lengths ranging from 25.4–88.9 cm, with the combustor step height unchanged. The schematic in Fig. 1 is for the 25.4 cm chamber. The longer combustor lengths produced unstable operation with peak-to-peak pressure oscillations greater than 25%, while the 25.4 cm combustor produced oscillations with peak-to-peak amplitudes of approximately 2%. The corresponding power spectral density (PSD) plot for the 25.4 cm combustor is shown in Fig. 1. Whereas measurements [23] for other combustor lengths showed magnitudes above 10^3 kPa^2/Hz, the 25.4 cm combustor showed peak magnitudes around only 10 kPa^2/Hz. The dominant unstable frequency for the 25.4 cm combustor occurs at 1905 Hz, which corresponds to its 1L mode. The mean pressure was around 2.38 MPa.

In an attempt to increase the coupling between acoustic pressure oscillations and the combustion heat release, a later test was performed [25] in which the backstep height adjacent to the injector face was decreased from 1.095 to 0.76 cm. The combustor radius in the initial experiments was constant at 2.25 cm throughout the entire combustor length, corresponding to an area of 0.159 cm^2. In the latter test, as shown in Fig. 3, the radius near the combustor face was at a smaller value of 1.905 cm and then was linearly increased near the midpoint of the combustor until it reached the previous value of 2.25 cm. This enabled the same nozzle to be used for both experiments. The 1.905 cm radius section of the combustor corresponds to an area of 0.114 cm^2. The reason for reducing the chamber step height was to enable vortices from the injector to impinge on the wall at a time when they amplified flame disturbances more strongly:, i.e., during a local compression. The experimental configuration and the resulting power spectral density of the measured pressure fluctuations for this modified combustor are shown in Fig. 3.

As demonstrated by PSD results on the right side of Fig. 3, the decrease in combustor step height resulted in much stronger oscillations with peak-to-peak pressure amplitudes increasing from 2% to 30–50%. The dominant mode now occurs at 2045 Hz. For this smaller-step-height chamber, the peak power magnitude is larger than 10^3 kPa^2/Hz, more than two orders of magnitude greater than the larger-step-height value (compare with Fig. 1). Reducing the step height near the injector face by 30% caused the peak-to-peak pressure oscillations to increase by an order of magnitude. This dramatic change was attributed to increased coupling between the dynamic pressure and the heat release caused by a change in the time required for the unsteady vortices to impinge on the closer wall in the smaller-step-height chamber [25,28]. Analyses of these two 25.4-cm-long combustors with different step heights are explored in the computational simulations that follow in an attempt to investigate whether CFD models can predict similar behavior and if CFD results agree with the experimentally observed trends.

B. Computational Model

The computations are conducted with an in-house unstructured grid code known as the General Equation and Mesh Solver (GEMS) code [29,30]. The GEMS code solves the Navier-Stokes equations in conjunction with the continuity and energy equations, pertinent species equations, and a turbulence model described below. The numerical procedure uses a second-order approximate Riemann solver to evaluate the spatial fluxes at cell faces. Second-order temporal accuracy is achieved by means of an implicit dual-time procedure that eliminates factorization errors. The computation of high Reynolds number, high Damkohler number, two-phase reacting flows of the present type represents a challenging computational problem. Because of these challenges, a number of approximations have been made, as outlined below.

The combustion process is incorporated by means of a four-species, single-step, finite rate global reaction for $C_{12}H_{23}$ and O_2 that is given as

$$4C_{12}H_{23} + 71O_2 \Rightarrow 46H_2O + 48CO_2 \quad (1)$$

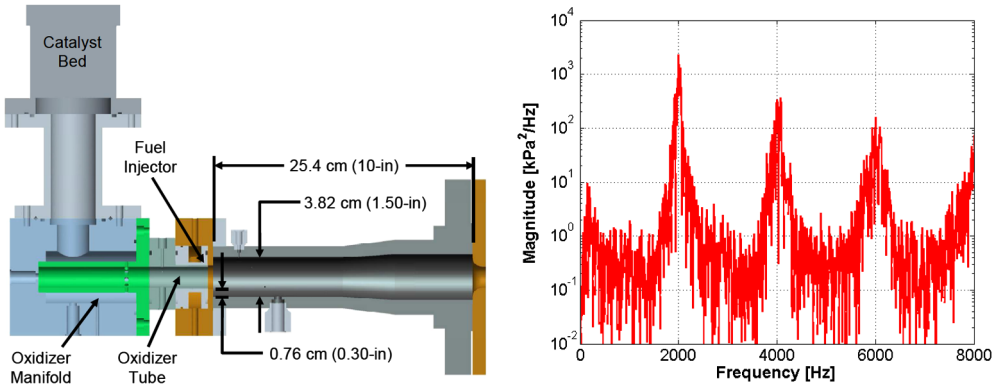

Fig. 3 Configuration of the modified 25.4 cm (10 in.) combustor experiment (left) and PSD plot showing a highly unstable response (right) [25].

This global expression replaces the highly complicated reaction of JP-8 fuel. To further simplify the analysis, the fuel was modeled as a vapor represented by the perfect gas law, thereby avoiding the need for atomization and vaporization models. The thermodynamic properties of both fuel and oxidizer and the equilibrium conditions for the reaction were obtained from the CEA computer code.[¶] These conditions were then input into the global reaction model to approximate the proper combustion temperature and molecular weight.

The mixing and combustion dynamics were simulated by a DES-like model in two dimensions that computes the large scales directly, and the smaller scales were treated by a RANS model. The underlying formulation for the small scales is the two equation k-ω turbulence model [31]. In boundary-layer and near-wall regions the k-ω model is used in unmodified form, while in regions where large scales can exist, the dissipation term in the turbulence model is diminished according to the ratio between the length scale obtained from the k-ω model and the local grid size [27,32]. The specific form of the modified dissipation term is

$$D_k = \frac{\rho k^{3/2}}{\tilde{l}} \tag{2}$$

where k is the turbulence kinetic energy and $\tilde{l}$ is the DES length scale. The DES length scale is defined as

$$\tilde{l} = \min(l_{k\text{-}\omega}, C_{\mathrm{DES}}\delta) \tag{3}$$

where δ is interpreted as the maximum grid spacing in any direction, i.e., $\delta = \max(\Delta x, \Delta y, \Delta z)$, and $l_{k\text{-}\omega}$ is the turbulence length scale in the k-ω turbulence model. C_{DES} is the constant coefficient in the DES model. All species are solved directly and the turbulent species transport is modeled by the classical gradient assumption with a constant turbulent Schmidt number for all species. Laminar reaction is used, assuming the reaction rate plays a minor role in the high Damkohler number flows in the present work. The computational grid was resolved to $y+ = 1$ at all walls such that no extra treatment of nonslip boundaries is necessary. All walls are assumed to be adiabatic.

The two-dimensional representation provides a first approximation to the dynamics of the large-scale fluctuations and helps to identify key phenomena at reasonable computational cost. Because it is two-dimensional, however, it omits vortex-stretching effects. There are several reasons for restricting the analysis to two dimensions. First, the Reynolds numbers of interest are high, with step-height Reynolds numbers on the order of 100,000. Wall boundary layers and near-wall effects are expected to play an important role in the analysis. Second, the recirculation regions created by the backstep height plus the long combustor length suggest that long simulation times will be required. Third, there appear to be no previous attempts at predicting self-sustained oscillations in a nonpremixed combustor of this type and there is some uncertainty as to whether or not such oscillations will be observed. Consequently, multiple computations are required to identify pertinent parameters as noted below. The two-dimensional formulation, therefore, helps to reduce computational costs and to increase the probability of success while enabling grid resolutions that cannot easily be duplicated in three dimensions. The grid sizes used for the present computations are 340,000 cells, and the corresponding simulation times have been computed for a duration of 100 ms. All calculations were run in parallel on a commodity cluster using nominally 50 to 100 processors.

Some additional approximations were also incorporated in the simulations with regard to the manner in which the reactants were injected into the chamber. In the experimental configuration, the oxidizer was injected radially through four holes spaced around the periphery of the oxidizer post at an axial location approximately midway along the post as shown in Fig. 2. A closed end was placed at the upstream end of the oxidizer post. This individual hole pattern cannot be duplicated in an axisymmetric model (and requires considerable grid allocation in three dimensions) but introduces an unknown level of upstream disturbances into the flowfield. To provide an appropriate level of upstream disturbances, four different oxidizer inflow conditions were considered, although detailed results for only two of these oxidizer inlets are presented.

Of the two oxidizer-inlet configurations presented in detail in the paper, the first uses axial, subsonic inflow to represent the incoming oxidizer. The subsonic inflow results in a smooth, uniform inlet stream that produces a minimum of upstream disturbances and low-level excitation in the chamber. The second oxidizer-inlet configuration is a slotted, choked orifice plate that isolates the combustion chamber from the upstream plenum. The flow downstream of the choked slots first expands supersonically before shocking to subsonic velocities to fill the full volume of the oxidizer post. The resulting shock pattern is highly unsteady and produces a series of disturbances that propagate into the combustor and increase the amplitude of oscillations to levels near those observed in the experiments. In the third inflow specification, the individual radial holes in the experiment were replaced by injection through an equivalent slot at the appropriate axial location in the oxidizer post. While this inlet allows the hard-wall upstream boundary condition to be included, the radial slot is a very poor representation of individual hole injection, and results for this boundary condition are not presented. The fourth inflow condition involved a choked plug nozzle, with the oxidizer entering through the annulus between the plug and the oxidizer-post wall. This injection condition again allowed the oxidizer to enter in supersonic fashion, followed by a normal shock train to subsonic conditions, and was used to understand mechanisms acting in the slotted inlet. This configuration resulted in the strongest upstream fluctuations, with oscillation amplitudes larger than those in the experiments.

These approximations allow a focus on identifying how well detailed computational models replicate observed experimental instabilities while also providing further insight into the measurements. As seen below, the predicted stability simulations provide proper qualitative trends and identify a number of key sensitivities in the modeling that are useful for additional studies. These results are also helpful in enhancing our understanding of instability mechanisms in the experiments.

III. Results

A. Computational Geometry and Initial Conditions

The computational domains for the two combustor geometries are compared in Fig. 4. This figure corresponds to the subsonic inlet. Details of the choked inlet are given later. The radius of the larger-step-height (1.095 cm) chamber in the top schematic is constant, while the radius of the smaller-step (0.76 cm) configuration in the bottom schematic increases from 1.905 to 2.25 cm between 12.7 and 17.8 cm downstream of the backstep. It is important to note that the computational domain includes the full oxidizer post, the fuel inlet passage (which is visible as the thin line just before the backstep into the combustor), the entire chamber, and enough of the nozzle to ensure that the flow remains choked during the anticipated pressure fluctuations. Each domain has 340,000 grid points.

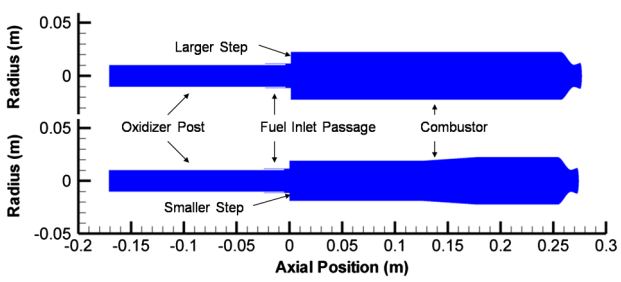

Fig. 4 Computational domains with uniform axial inlet for the larger-step-height combustor (top) and the smaller-step-height combustor (bottom).

[¶]Data available online at http://www.grc.nasa.gov/WWW/CEAWeb/ [retrieved 14 September 2007].

Although our interest lies with deducing the magnitude of stationary fluctuations inside the combustor, it is important to specify the initial condition from which the computations were obtained. All simulations were started from quiescent conditions inside the chamber and injector passages. The respective injector passages were filled with fuel and oxidizer over most of their length, and a small portion near the chamber and the chamber itself were filled with hot, quiescent CO_2. The initial pressure inside the entire domain was set to the experimentally measured chamber pressure. At time zero, flow was initiated by breaking a diaphragm at the exit plane exposing the exit plane of the nozzle to a low backpressure to choke the flow and simultaneously initiating the specified mass flow rates of fuel and oxidizer through their respective upstream ports. The diaphragm at the downstream end allowed an expansion wave to enter the chamber, initiating flow through the nozzle. The incoming mass flow at the upstream boundaries generated weak shocks that propagated through the respective propellant passages and into the chamber, likewise initiating flow from the upstream end. As the fuel and oxidizer in the inlet passages were transported into the chamber and came into contact with each other, the hot CO_2 provided sufficient energy for spontaneous ignition and combustion. This computational ignition proved to be both reliable and smooth. The computations were continued for a sufficiently long time that the effects of this initial condition were removed from the flowfield, and stationary, unsteady conditions were reached. The dynamics of this initial transient are analogous to an initial forcing of the combustor and are interesting in themselves. Accordingly, some results during this initial transient are also reported. In addition a grid resolution study makes use of this initial transient.

B. Uniform Subsonic Oxidizer Inflow

The uniform subsonic inflow condition results in a smooth incoming flow with minimal disturbances introduced at the upstream end, apart from acoustic reflections of pressure waves generated inside the chamber and associated weak entropy waves. With this inlet, most of the vorticity in the flowfield is generated at the step between the fuel and oxidizer manifolds. Nevertheless, the long-term stationary flowfield in the combustor contains a substantial amount of unsteadiness.

In the current and subsequent sections, the results are presented as follows. First the pressure fluctuations at a particular point are shown for both the larger and smaller steps. This gives an indication of general characteristics and trends, including any growth or decay and the relative amplitudes of the two cases. The pressure oscillations are then investigated further by performing PSD analysis, which gives an indication of how much of the pressure signal coincides with chamber acoustics. The coupling between unsteady pressure and heat release is then compared both visually and quantitatively by calculating the Rayleigh index. This gives an indication of whether the observed results correspond to combustion instability, or are simply flow oscillations. The axial distributions of mean pressure and mean heat release are also presented for reference.

A first insight into system operation can be gained from the global time history of chamber pressure in Fig. 5, which shows pressure traces for both the larger- and smaller-step-height chambers over two time intervals. These pressure traces correspond to a location on the combustor wall 1.27 cm downstream of the backstep, which is near a pressure antinode of the first longitudinal mode and matches a transducer location in the experiment. This location also corresponds to a region where a large amount of reactants is available for combustion and therefore a potential region of high heat release, suggesting that it is a key location for investigating instability phenomena. The plot on the left of Fig. 5 shows the long-term history of the pressure fluctuations from 0 to 80 ms, and the one on the right shows early time details from 2 to 16 ms.

Upon initiation, the chamber pressure in both geometries overshoots with peak-to-peak oscillations reaching 0.7 MPa, before settling down to levels of approximately 0.2 MPa, corresponding to an approximate peak-to-peak fluctuation of 10% of the 2.1 MPa mean pressure. The peak-to-peak oscillations in the larger-step-height combustor are equal to or lower than those in the smaller-step-height combustor. The more detailed plot on the right of Fig. 5 indicates that the disturbances in the chamber with the larger step decay considerably more rapidly than those in the smaller-step-height chamber (compare solutions between 5 and 10 ms), a first indication that the step height does affect the pressure oscillations in the simulations. Although this initial transient arises from the numerical startup procedure, it is analogous to the decay following an initial perturbation and the increased rate of decay in the larger-step-height combustor is an indication of its greater stability. Again, the plot on the left suggests that the long-term oscillations in the smaller backstep chamber remain modestly larger at longer times, but the disturbances are sufficiently small that a definite observation cannot be made.

As a check on grid convergence, the number of cells for the smaller-step-height-combustor case was halved in both directions, resulting in a grid of 87,500 cells: approximately one-fourth of the previous grid. The pressure fluctuations on this coarser grid are compared with those on the original grid in Fig. 6 for times between 0 and 40 ms. The comparison shows a difference during the initial transient but demonstrates reasonable agreement between the two solutions at later times. Similar acoustic modes were excited in both cases and the level of pressure fluctuations was roughly the same suggesting that the results are reasonably independent of grid.

Returning to the fine-grid results, the PSD results are given in Fig. 7. These provide an indication of which acoustic modes are being excited and the magnitude of the oscillations at these frequencies. The PSD analyses in Fig. 7 are again presented for two different time intervals. The first interval (on the left) is taken from 2

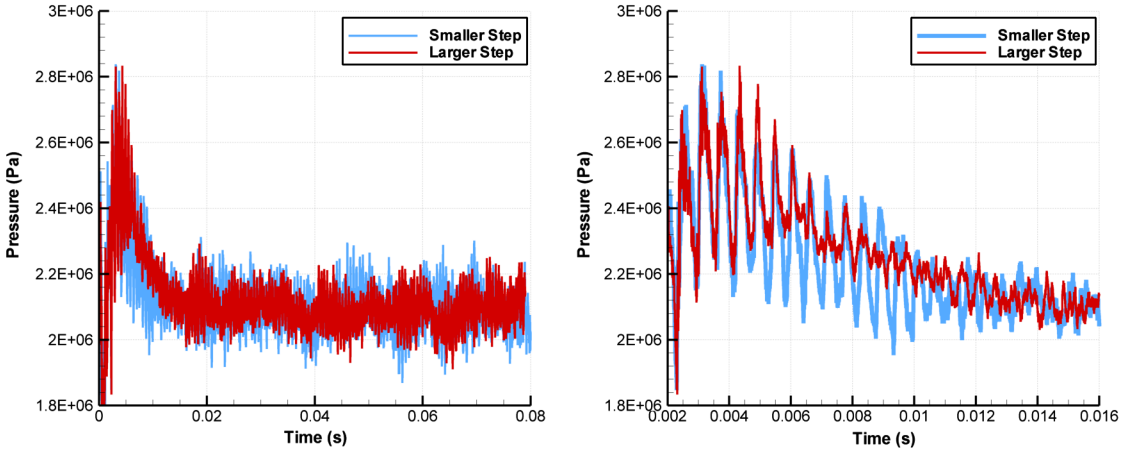

Fig. 5 Pressure trace from 0 to 80 ms (left) and from 2 to 16 ms (right) for the larger-step-height combustor and the smaller-step-height combustor. Uniform subsonic inflow.

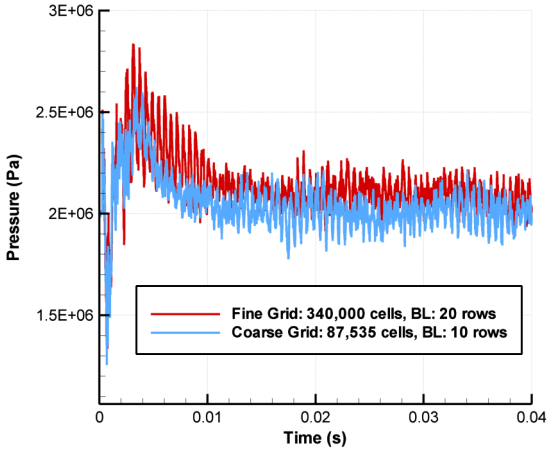

Fig. 6 Effect of grid refinement on pressure history: Fine grid, 340,000 cells; Coarse grid, 88,000 cells. Smaller-step-height combustor; uniform subsonic inflow.

to 12 ms which allows a maximum frequency resolution of 100 Hz. During this early interval, the first and second longitudinal modes (1700 and 3500 Hz) of the smaller-step-height combustor have noticeably larger amplitudes than those of the larger-step-height combustor, as anticipated from the pressure–time plots.

The PSD plot on the right side of Fig. 7 is taken over the interval from 15 to 80 ms allowing a frequency resolution of 15 Hz. This shows the first longitudinal mode occurring at about 1750 Hz. During this time interval, there is only a small difference between the two step-height configurations. The amplitude of the pressure fluctuations observed in the experiment is clearly not captured for the subsonic uniform inlet case.

A quantitative interpretation of the coupling between the unsteady heat release and the oscillating pressure can be obtained from the Rayleigh index, which is defined as the temporal integral of the product of the unsteady pressure p' and the unsteady heat release Q' over a specified time interval, t:

$$\int_0^t p'(t) \cdot \dot{Q}(t) \cdot \mathrm{d}t \tag{4}$$

The Rayleigh index is a mathematical expression of Rayleigh's criterion, which states that when heat release and pressure oscillations are in phase, the pressure will be amplified and when they are out of phase the pressure will be damped [33,34]. The time history of the Rayleigh index calculated over 1 ms intervals and integrated over the entire combustor volume is plotted in Fig. 8 for the present subsonic-inlet simulation. Although there are strong fluctuations at the outset of the calculation, the Rayleigh indices of both step-height combustors decay to relatively small values at later times, in agreement with the earlier PSD evaluations that show relatively low-amplitude disturbances. The smaller step appears to generate larger Rayleigh indices, although the differences are small after the first 10 ms. During the first 10 ms of the simulation, however, when disturbances in the chamber are responding to the perturbation caused by the initial conditions, the Rayleigh index for the smaller-step-height combustor is decidedly larger than that for the larger step, indicating higher coupling in the smaller-step combustor.

The axial distribution of the pressure and heat release integrated across the cross section of the combustor and time-averaged between 15 and 80 ms is presented in Fig. 9 for both step-height chambers. The zero location corresponds to the location of the step and the 25.4 cm location corresponds to the entrance to the nozzle. The chamber pressures for the two cases are nearly identical and are about 12% lower than the experimental values. The mean heat release for the smaller-step-height combustor is slightly larger than for the larger-step-height combustor, again indicating stronger coupling with the smaller step, but overall they are quite similar. Also note that heat release occurs throughout the entire length of the combustor and into the nozzle.

C. Choked Upstream Boundary-Condition Simulations

The upstream boundary condition used in the simulations of the previous section results in nearly uniform subsonic flow near the inlet (the Mach number is approximately 0.3) that gives rise to relatively low disturbances and small chamber oscillations. This boundary condition failed to reproduce the substantial disturbances generated by the multiple radial jet injection used in the experiments. A further difficulty with any subsonic inlet is that accurate simulations require modeling the complete inlet manifold to properly represent upstream disturbance reflections. The radial inlets used in the experiments were also subsonic, however, and would not only require detailed three-dimensional resolution, but would also require modeling the inlet manifold. Finally, an assessment of the sensitivity of the CFD predictions to the upstream boundary condition was warranted. Accordingly, a choked upstream boundary condition was chosen to provide a clean unsteady boundary condition for simulations while also serving as a model for future experiments designed for CFD validation. It was also anticipated that a choked inlet would act as a hard boundary that would reflect upstream propagating disturbances in a manner somewhat analogous to a solid wall and would thus be more representative of the experiment.

The first choked upstream geometry considered was a converging–diverging nozzle. For experimental purposes, a plug nozzle was more attractive than a conventional nozzle, and the configuration shown in Fig. 10 was analyzed. The computational domain extended from upstream of the first choked throat (where the mass flow rate and a uniform stagnation temperature were specified as boundary conditions) through a second choked nozzle downstream of the combustion chamber. As the results in Fig. 10 show, the flow downstream of the choked plug nozzle is highly nonuniform, with large axial and radial variations that were strongly unsteady in

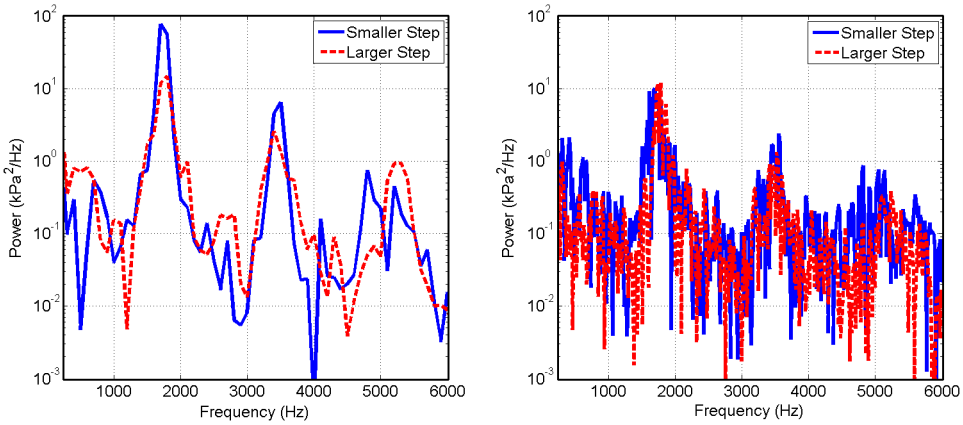

Fig. 7 PSD plots from 2 to 12 ms (left) and from 15 to 80 ms (right) for the larger-step-height combustor (dashed line) and the smaller-step-height combustor (solid line). Uniform subsonic inflow.

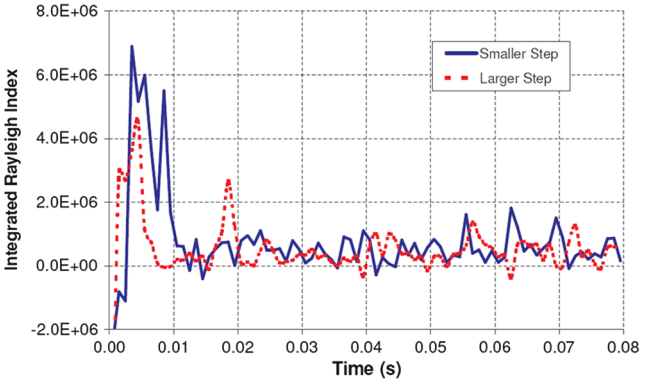

Fig. 8 Axially integrated Rayleigh index for the uniform axial subsonic inlet for the larger-step-height and smaller-step-height combustors.

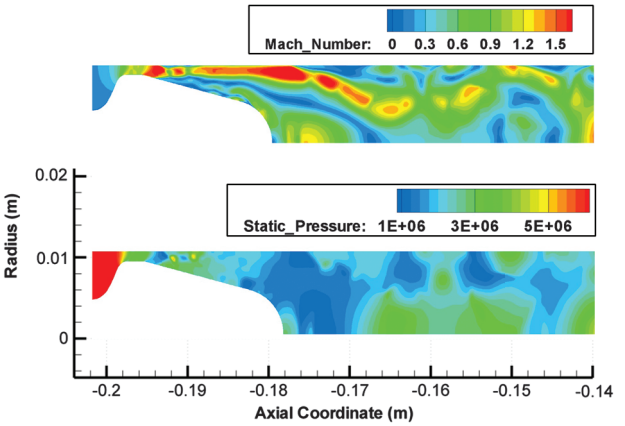

Fig. 10 Geometry of choked plug nozzle showing Mach number contours with streamlines (top) and pressure contours (bottom).

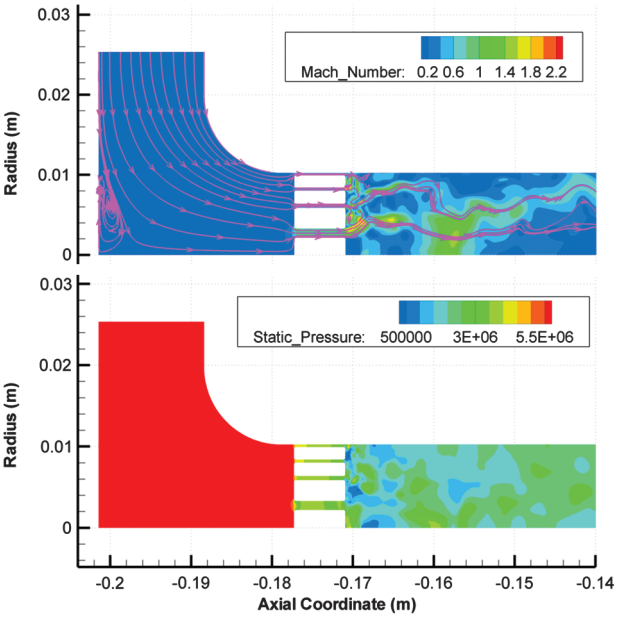

Fig. 11 Mach number plot with streamlines (top) and pressure plot (bottom) showing radial injection with the choked slot inlet.

character. Instead of simply acting as a choked throat when the Mach number was unity, the flow in the divergent section initially expanded to supersonic speeds before shocking to subsonic speeds to give the appropriate entropy to allow simultaneous choking at the second chamber nozzle downstream. The shock/boundary-layer interaction accompanying this process resulted in unsteady shock fluctuations and the divergent portion of the plug responded much like the isolator in a hypersonic inlet, with a shock train that translated back and forth in time in response to pressure fluctuations in the chamber. Although the choked throat provides isolation from the upstream plenum, the unsteady flow and entropy generation in the mixed supersonic/subsonic flow downstream of the slots creates a complex, but readily simulated, acoustic boundary condition at the upstream end. This is in contrast to the general expectation that choked boundaries provide very simple upstream boundary conditions. The pressure fluctuations generated by the choked plug nozzle resulted in larger chamber oscillations than seen in the experiment, giving clear proof that the upstream boundary configuration plays an important role in instability simulations.

The slotted choked orifice plate was chosen as a compromise between the strong instabilities generated by the choked C-D nozzle and the very benign (and poorly defined) upstream conditions observed in the subsonic inlet. The geometrical configuration of the slotted orifice plate is shown in Fig. 11 in conjunction with the instantaneous Mach number and static pressure contours. To reduce the level of fluctuations, four slots were used in the orifice plate to decrease the length scale of the now expected fluctuations from the unsteady shock patterns. The resulting decrease is clearly seen by comparing Figs. 10 and 11. The plug-nozzle simulations clearly demonstrate the necessity of starting upstream of the choke location. A simple Mach 1 upstream boundary specification cannot be used. Accordingly, the mass flow and stagnation temperature were again specified upstream of the orifice plate. As Fig. 11 shows, the subsonic stream was introduced radially. The sonic region, however, isolates the inlet from downstream disturbances so the actual geometry used in the upstream region is immaterial.

The choked, slotted inlet simulations have been run for a total time of 100 ms. The present discussion focuses on the final 30 ms of the simulations after stationary conditions have been established. pressure–time fluctuations between 70 and 100 ms are shown in the left plot of Fig. 12 for both step-height chambers, and fluctuations over the interval from 90 to 95 ms are given in the plot on the right. For clarity, the short-term trace on the right shows results for only the

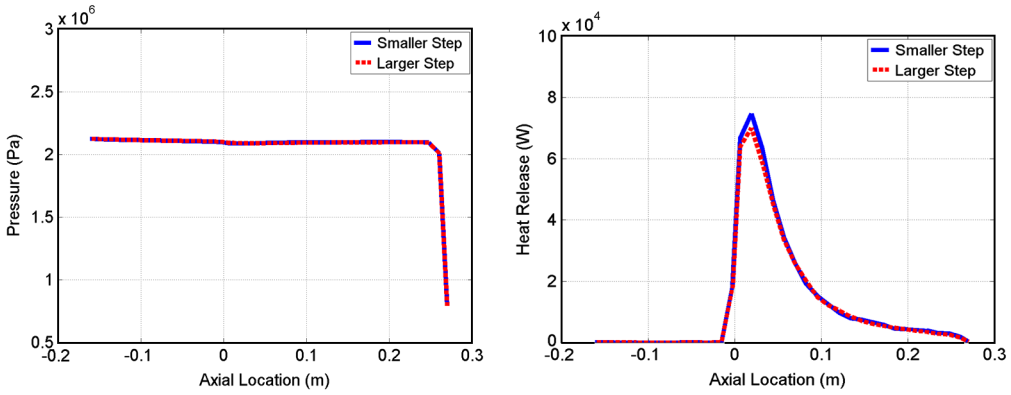

Fig. 9 Mean pressure distribution (left) and mean heat-release distribution (right) between 15 and 80 ms for both combustors. Uniform subsonic inlet.

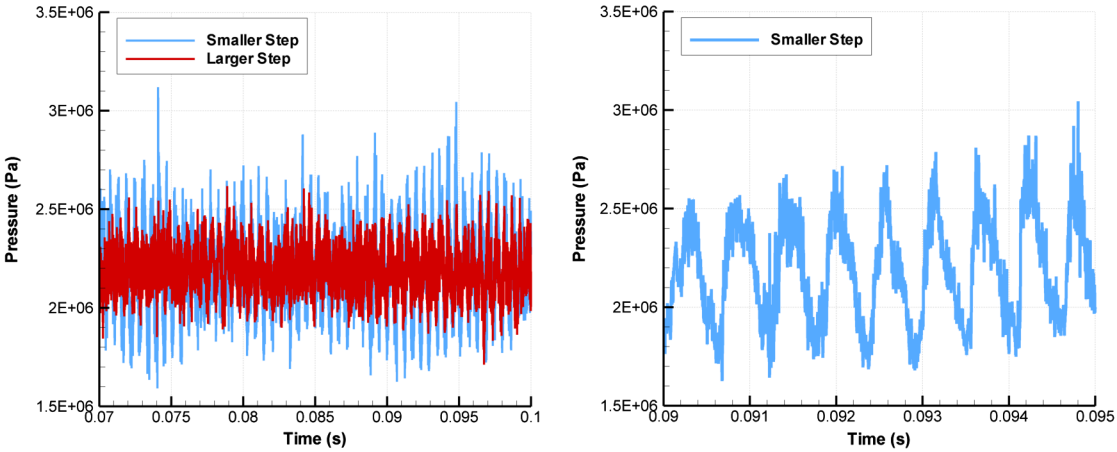

Fig. 12 Global pressure time trace between 70 and 100 ms for both combustors (left) and local fluctuations between 90 and 95 ms (right) for the smaller-step configuration. Slotted inlet simulation.

smaller step height. The location of the pressure probe is again 1.27 cm downstream of the step. Comparison with Fig. 5 shows that the choked-inlet results have substantially higher pressure fluctuations. It is also clear from Fig. 12 that the fluctuations produced by the smaller step height are noticeably larger than with the larger step height when the slot inlet is used. The pressure trace for the smaller-step-height case (right side of Fig. 12) shows steep-fronted waves at the first longitudinal mode frequency.

PSD plots for the choked-inlet simulations are presented in Fig. 13. The PSD in the left plot is based on results between 70 and 100 ms (which enables a maximum frequency resolution of 33 Hz), and the plot on the right corresponds to the interval between 90 and 100 ms (which allows 100 Hz resolution). Note that the scale in both plots is two orders of magnitude greater than that in Fig. 7 and the peak magnitudes are correspondingly higher. In agreement with the pressure plots, the magnitude of the fluctuations produced by the smaller step is generally higher than that from the larger step. This is especially true for the first longitudinal mode (between 1733 and 1800 Hz, depending on the resolution), in which the power magnitude peak is almost a factor of 10 higher.

The PSD plot on the right for the shorter interval shows that the second longitudinal mode (the first higher harmonic, 3500 Hz) is also noticeably higher for the smaller step height than for the larger step height. These observations are consistent with the trends of the experimental PSD plots (Fig. 3), in which the smaller-step combustor showed higher power magnitudes than the larger-step combustor. For both the smaller- and larger-step combustors, the highest peaks tend to occur around the acoustic frequencies. This verifies that the pressure fluctuations are predominately acoustic in nature and not just noise generated by disturbances from the oxidizer post.

Further understanding can be gained by analyzing the coupling between heat release and pressure oscillations. For this purpose the heat release and pressure have been integrated over the segment of the combustor from 1.27 to 2.54 cm downstream of the step as a function of time. These time histories are plotted in Fig. 14 for both chambers, with the results for the larger step on the left and the smaller step on the right. The darker lines in both plots represent the unsteady heat release, and the lighter lines represent the unsteady pressure in this volume. The pressure and heat-release values have been normalized so that they could be plotted on a common scale.

The heat release and pressure fluctuations in the smaller-step-height combustor are mostly in phase with the peaks in heat release largely coinciding with the peaks in pressure. For the larger step, the heat-release peaks are more broadly distributed over time and the pressure peaks are less steep-fronted. There still appears to be correspondence, but it is considerably less pronounced than for the smaller step height, again suggesting that the heat-release/pressure coupling is stronger for the smaller-step-height combustor.

A plot of the Rayleigh index as a function of axial location, calculated over the interval from 93 to 94 ms, is shown in Fig. 15, with the solid line representing the smaller-step-height combustor and the dashed line representing the larger-step-height combustor. The 1 ms integration time in Fig. 15 corresponds to approximately $1\frac{3}{4}$ of a cycle of the first longitudinal mode (compare with Fig. 14). The plot shows a much higher Rayleigh index for the smaller-step combustor than for the larger-step combustor between 0 (the step location) and 100 cm downstream. Note that the oscillating pressure is high in this region due to the pressure antinode. In addition, there is a large concentration of unburned reactants available for combustion in this region. This allows for potentially large unsteady pressure/

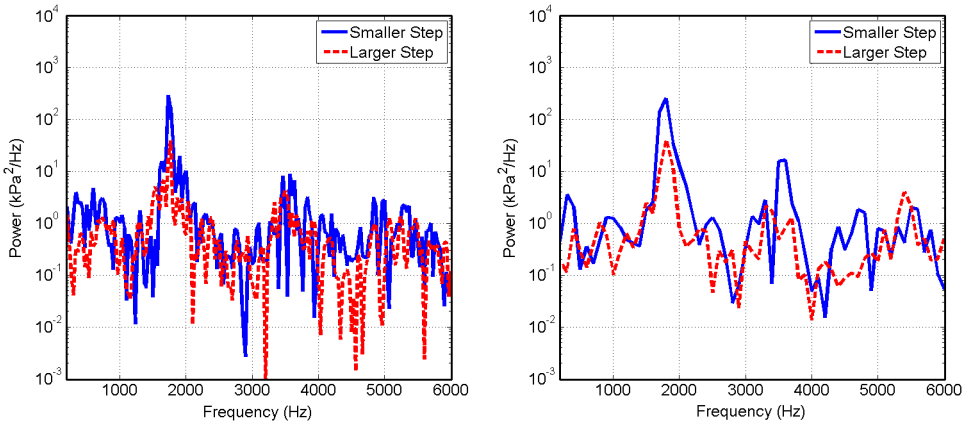

Fig. 13 PSD plots from 70 to 100 ms (left) and from 90 to 100 ms (right) for the larger-step-height (dashed line) and the smaller-step-height (solid line) chambers. Slotted inlet.

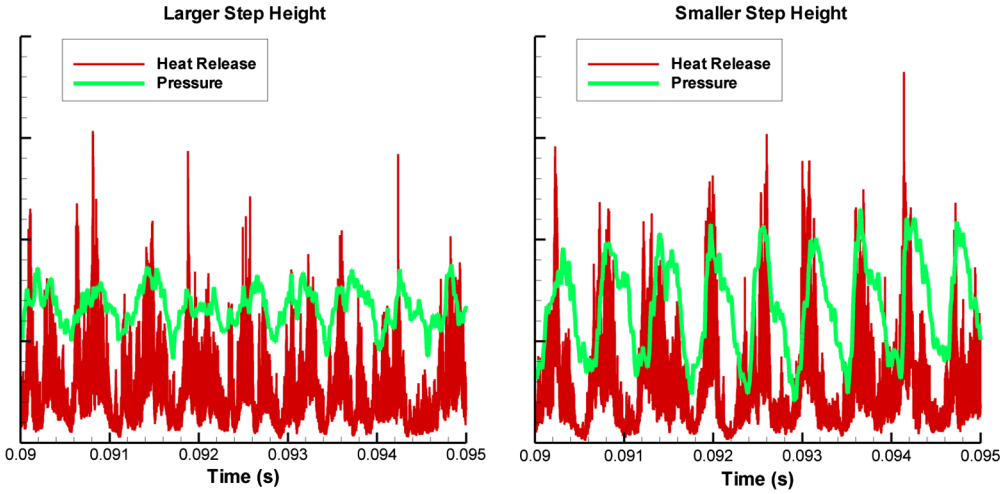

Fig. 14 Plots of heat release and pressure from 0.090–0.095 s for the larger-step-height combustor (left) and the smaller-step-height combustor (right). Slotted inlet.

heat-release coupling. The peak Rayleigh index for the smaller-step-height combustor occurs at 0.032 m.

The time history of the axially integrated Rayleigh index for the choked inlet is shown in Fig. 16 for the time interval between 70 and 100 ms. The Rayleigh index for the smaller-step-height combustor is consistently higher than that for the larger step height, again indicating larger pressure/heat-release coupling for the smaller step height. Since the PSD plots in Fig. 13 demonstrated the acoustic nature of the pressure oscillations, the difference in pressure oscillations between the two step-height cases is likely due to this difference in coupling. Thus, the pressure time traces, the PSD plots, and the Rayleigh index all indicate a higher level of combustion instability for the smaller step height than for the larger step height, in agreement with the trends of the experiment. The oscillations clearly appear to be self-sustaining as this difference has been maintained over 30 ms, corresponding to more than 50 cycles of the first longitudinal mode. The choked-inlet results, therefore, indicate that the unsteady heat release can be sufficiently well simulated to represent combustion instability behavior in CFD calculations.

Comparison of the choked-inlet results with the subsonic-inlet results in Fig. 8 shows the integrated Rayleigh index is substantially larger for the choked inlet than for the subsonic inlet (note that the scales are different in Figs. 8 and 16). For the smaller backstep, the peak amplitudes in the choked-inlet case exceed 20×10^6, while for the later 60 ms of the subsonic-inlet case, the peaks are below 2×10^6, more than a factor of 10 lower. For the larger backstep, the peaks for the choked inlet reach to about 5×10^6, and for the subsonic inlet they are approximately 1×10^6. This suggests that after the initial transient, the choked inlet is more unstable than the subsonic-inlet case and that the choked inlet amplifies the effect of the smaller backstep height on the interactions. The reasons for the difference are because of the more reflective upstream boundary condition with the choked inlet as well as the higher level of excitation. The difference in stability characteristics between the subsonic and choked inlets highlights the importance of boundary conditions and upstream disturbances both when modeling combustion instability and when designing laboratory experiments.

As a final look at the flow characteristics in the choked nozzle case, we compare in Fig. 17 the mean pressure and the mean heat-release distributions between the downstream side of the slotted orifice plate and the nozzle throat for the two different step heights. As for the subsonic inlet (Fig. 9) the mean pressures in the two chambers are very similar, with values around 2.2 MPa at the midpoint of the combustion chamber. This is about 5% higher than for the subsonic-inlet cases and about 7% lower than the experimental value. Note that the mean pressure increases as the flow moves through the oxidizer post, corresponding to deceleration of the flow.

The time-averaged heat release for the larger- and smaller-step-height cases is also quite similar, except that the smaller-step-height case shows a slightly higher peak heat release. The peak in the time-averaged heat release for the choked inlet is approximately 7% larger than for the subsonic-inlet case (again note that the scales are different in Figs. 9 and 17), indicating a more distributed heat release in the subsonic-inlet case. The stronger upstream disturbances in the choked-inlet case appear to concentrate the heat release closer to the backstep, in which it couples more strongly with the pressure oscillations, leading to stronger amplification. Also note that some

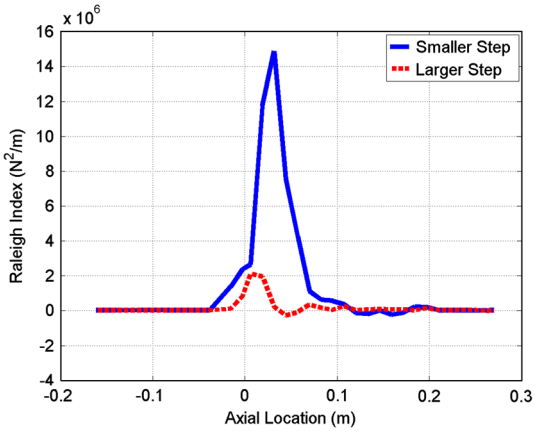

Fig. 15 Rayleigh index time-averaged over the interval from 93 to 94 ms. Larger-step-height (dashed line) and smaller-step-height (solid line) combustors. Slotted inlet.

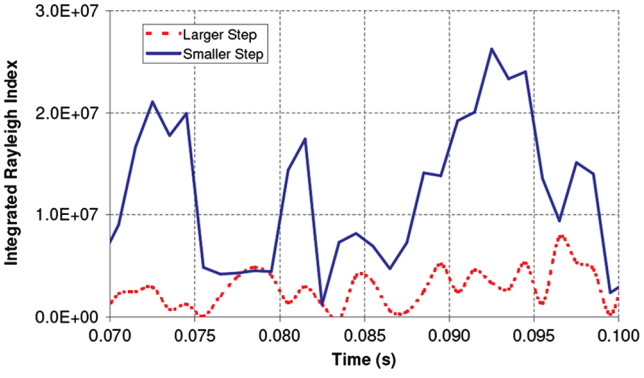

Fig. 16 Axially integrated Rayleigh index for the choked slot inlet for the larger-step-height and smaller-step-height combustors. Slotted inlet.

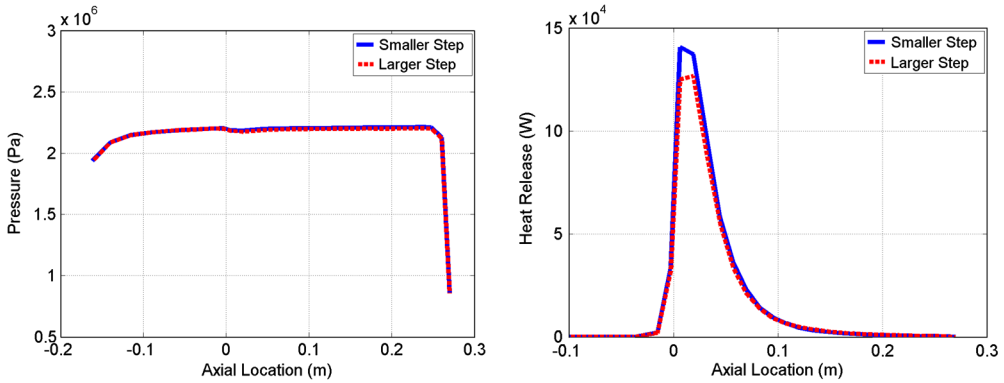

Fig. 17 Time-averaged pressure (left) and heat-release (right) distributions for both combustors. Choked inlet.

combustion occurs inside the oxidizer post upstream of the combustor for the choked-inlet case. This difference in mean heat release is attributed to the larger amount of upstream vorticity for the choked slot case, which causes enhanced mixing and the higher peak in the heat release.

D. Instantaneous Flowfield Patterns

The simulations have shown, in agreement with experiment, that the smaller-step-height combustor exhibits stronger pressure fluctuations than does the larger one. The instantaneous heat release and pressure traces are more nearly in phase and the Rayleigh index is larger for the smaller step, indicating that the stronger fluctuations arise from coupling between the combustion and chamber acoustics. Further insight into the causes of these differences can be obtained from the instantaneous flowfields. Because the stronger instabilities generated by the choked inlet cause the flow patterns to be more complicated, we start with results from the subsonic inlet for which the more uniform inflow allows vortex shedding from the step and eventual wall impingement to be visualized more easily.

Four consecutive snapshots, each 0.1 ms apart, of the instantaneous oxidizer mass-fraction contours in the vicinity of the backstep are presented in Fig. 18 for the larger-step-height chamber and Fig. 19 for the smaller step. Instantaneous streamline contours are shown at one time instant to provide further insight into the flow dynamics. The field of view starts upstream of the backstep and extends over the upstream half of the combustor.

The topmost plot in each figure shows a large vortex of high oxidizer concentration forming near the backstep. The three succeeding plots show the fate of this vortex as it moves downstream, mixes with fuel, reacts and releases heat. Note that near the step the vortices behind both steps appear very similar, although their ensuing trajectories are quite different. By the time the vortex from the larger step height (Fig. 18) approaches the wall, it has broken up considerably. The streamline patterns in the bottom plot show three vortices. The vortices appear to reach the wall approximately 5 cm (4.5 step heights) downstream of the step, after which they are convected downstream. By contrast, the vortex from the smaller-step-height chamber (upper plot of Fig. 19) impinges much sooner, approximately 2 cm (2.5 step heights) downstream of the step and exhibits a stronger interaction with the wall. The smaller step height causes the vortex to impinge on the wall earlier, and then subsequently to break up. These same nominal patterns are repeated intermittently throughout both simulations, suggesting that vortex impingement on the wall is important in driving the larger oscillations in the chamber with the small step. Comparisons of pressure and heat release with snapshots of the concentration distribution taken over a 10 ms window for the smaller-step-height combustor confirm that each heat-release spike corresponds to a vortex impinging on the wall. A similar visual/quantitative correspondence was not observed for the large-step combustor.

Details of the near-step flow dynamics produced by the choked inlet are given in Fig. 20. Again, concentration distributions are shown for four time instants, $t = 74.71$, 74.745, 74.78, and 74.815 ms, although here only the smaller-step results are shown. As with the subsonic inlet, these pictures provide evidence of vortex/wall impingement and breakup in the smaller-step-height combustor.

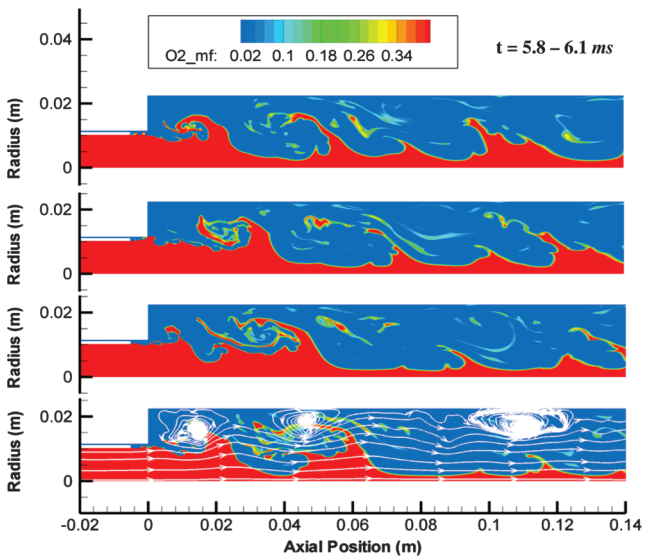

Fig. 18 Oxidizer mass-fraction plots for the larger-step-height combustor from 5.8–6.1 ms (only part of oxidizer passage and half of combustor shown). Subsonic inlet. Streamlines are shown in the last plot.

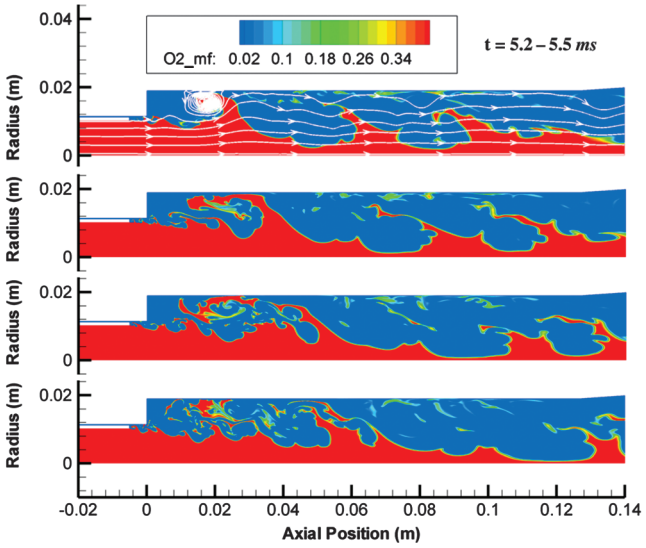

Fig. 19 Oxidizer mass-fraction plots for the smaller-step-height combustor from 5.2–5.5 ms (only part of injector and half of the combustor is shown). Subsonic inlet. Streamlines are shown in the first plot.

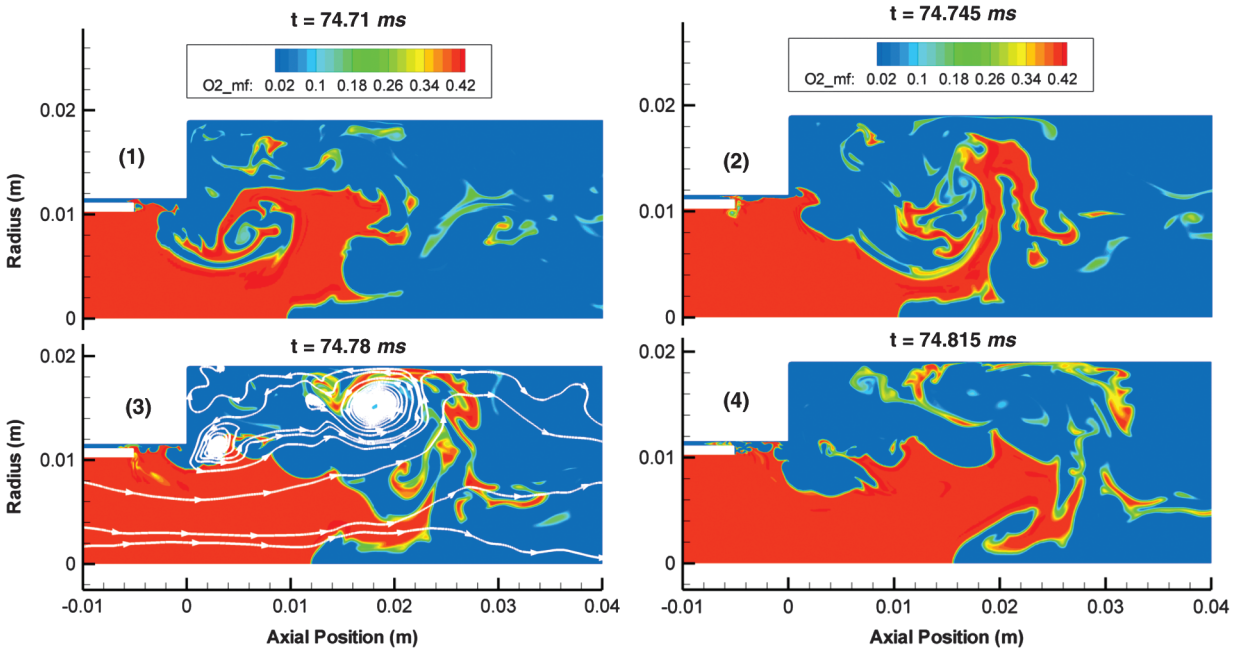

Fig. 20 Oxidizer mass-fraction plots for the smaller-step-height combustor from 4.5–4.8 ms (only part of injector and half of the combustor is shown). Choked inlet.

As noted above, the flow patterns generated downstream of the choked inlet are less organized than those for the subsonic inlet, but, in general, the increased upstream excitation and larger amplitude disturbances appears to cause the vortices to impinge closer to the backstep than for the subsonic inlet in Fig. 19. Comparing with Fig. 14, this vortex impingement mechanism also explains why the peak Rayleigh index occurs a few centimeters downstream of the step, even though the pressure antinode occurs at the step. Vortex impingement also occurs for the larger-step-height combustor, but the interactions are less frequent and less intense.

As a final point, the wall/vortex interaction shown above makes it clear that the level of instability will not continue to increase as the step height approaches zero. A zero step will produce no vortices, while a very large step will not allow vortex/wall interactions. Thus, an optimum step height for maximum instability likely exists. We have not investigated this optimum, but have restricted computational configurations to the experimentally tested step heights.

IV. Conclusions

Time-accurate simulations of the mixing and combustion in a high-pressure combustor supplied by independent fuel and oxidizer feed streams have been conducted to investigate the potential for using CFD to represent high-frequency combustion instability. The formulation is based upon an approach analogous to DES that models large-scale structures directly while still retaining capability for integration to the wall in turbulent boundary layers. For computational efficiency the simulations were limited to two dimensions to enable high-resolution grids, long simulation times, and multiple cases. Companion experiments were used to identify stable and unstable regions and to test whether the CFD procedure could predict pertinent trends. A major uncertainty was whether direct simulation of large-scale structures was sufficient to generate self-induced oscillations or whether all disturbances in the computation would eventually decay to zero.

The focus of the paper concerns the effects of changes in the backstep height of a dump combustor. Experiments have shown over an order of magnitude increase in self-induced oscillation amplitudes for a 30% change in the backstep. The simulations predict a similar trend: the smaller backstep produces larger oscillation amplitudes than the larger one. Simulations with a subsonic oxidizer-inlet stream decayed to relatively low levels as compared to the experiments, but indicated faster decay for the larger step during the initial transient. Simulations based upon a choked-oxidizer-inlet stream produced long-term oscillations with amplitudes similar to experimental ones and, in addition, agreed with the experiment by showing stronger oscillations with the smaller step.

The impact of the upstream boundary condition was shown to arise because of the level of disturbances generated by the incoming flow. The experimental installation generated disturbances through multiple radial injection holes. The subsonic inlet resulted in very low-level disturbances in the incoming oxidizer stream, while the choked inlet led to supersonic expansion followed by transient shock-wave/boundary-layer interactions that generated vorticity and entropy fluctuations. The increased unsteadiness resulted in more rapid mixing and heat release and served as a trigger for acoustic mode amplification in the region of the backstep and indicates that care must be exercised in defining experimental models for instability testing as well as in setting up computational simulations of them.

Detailed information was obtained from the simulations by comparing Rayleigh indices, power spectral density plots, the phase relationship of local unsteady heat release and pressure oscillations, and instantaneous flowfield contours. The PSD analyses confirmed the presence of acoustic modes, with significantly higher acoustic pressure oscillations for the smaller step than for the larger one. Rayleigh index calculations also showed significantly higher values for the smaller-step combustor, demonstrating that the local unsteady heat release was more strongly in phase with the unsteady pressure. In addition, the time-averaged heat release in the vicinity of the step was notably larger for the smaller-backstep choked-inlet case, indicating more potential for pressure/heat-release coupling. Visualizations of the instantaneous flowfield indicated stronger vortex/wall interactions with the smaller backstep height.

Overall, the results indicate that the unsteady heat release generated by the large-scale dynamics can, indeed, drive self-sustained oscillations. The fact that these results are in agreement with experimental trends suggests that CFD simulations represent a very important complement to model experiments in combustion instability studies. Clearly, the three-dimensional effects that have been omitted here are important in any such detailed unsteady analyses, but the present results suggest that two-dimensional results serve as an excellent guide for the more computationally intense 3-D simulations.

Acknowledgments

This research was sponsored by the NASA Constellation University Institutes Project (CUIP). Most of the computations were run on the NASA Columbia supercomputer. The authors would like to thank Claudia Meyer and Jeff Rybak of NASA John H. Glenn Research Center at Lewis Field for their support. Technical advice was also received from, and appreciation is expressed to, Enrique Portillo, Jim Sisco, and Yen Yu of Purdue University.

References

[1] Harrje, D. T., and Reardon, F. H. (eds.), *Liquid Propellant Rocket Combustion Instability*, NASA SP-194, Washington, D.C., 1972.

[2] Oefelein, J. C., and Yang, V., "Comprehensive Review of Liquid-Propellant Combustion Instabilities in F1 Engines," *Journal of Propulsion and Power*, Vol. 9, No. 5, Sept.–Oct. 1993, pp. 657–677. doi:10.2514/3.23674

[3] Yang, V., and Anderson, W. E. (eds.), *Liquid Rocket Engine Combustion Instability*, AIAA, Washington, D.C., 1995.

[4] Culick, F. E. C., and Yang, V., "Overview of Combustion Instabilities in Liquid-Propellant Rocket Engines," *Liquid Rocket Engine Combustion Instability*, edited by V. Yang, and W. E. Anderson, AIAA, Washington, D.C., 1995, Chap. 1.

[5] Culick, F. E. C., "Combustion Instabilities in Liquid-Fueled Propulsion Systems—An Overview," AGARD, CP-450, Neuilly-sur-Seine, France, 1989.

[6] Zinn, B. T., "A Theoretical Study of Nonlinear Combustion Instability in Liquid Propellant Engines," *AIAA Journal*, Vol. 6, No. 10, 1968, pp. 1966–1972. doi:10.2514/3.4908

[7] Yang, V., Wicker, J. M., and Yoon, M. W., "Acoustic Waves in Combustion Chambers," *Liquid Rocket Engine Combustion Instability*, edited by V. Yang, and W. E. Anderson, AIAA, Washington, D.C., 1995, Chap. 13.

[8] Dowling, A. P., and Stow, R. S., "Acoustic Analysis of Gas Turbine Combustors," *Journal of Propulsion and Power*, Vol. 19, No. 5, 2003, pp. 751–763. doi:10.2514/2.6192

[9] Mitchell, C. E., "Analytical Models for Combustion Instability," *Liquid Rocket Engine Combustion Instability*, edited by V. Yang, and W. Anderson, Vol. 169, Progress in Astronautics and Aeronautics, AIAA, Washington, D.C., 1995, Chap. 15.

[10] Pierce, C. D., and Moin, P., "Large Eddy Simulation of a Confined Coaxial Jet with Swirl and Heat Release," 29th AIAA Fluid Dynamics Conference, Albuquerque, NM, AIAA Paper 1998-2892, June 1998.

[11] Menon, S., and Jou, W., "Large-Eddy Simulations of Combustion Instability in an Axisymmetric Ramjet Combustor," *Combustion Science and Technology*, Vol. 75, 1991, pp. 53–72. doi:10.1080/00102209108924078

[12] Martin, C., Benoit, L., Sommerer, Y., Nicoud, F., and Poinsot, T., "Large Eddy Simulation and Acoustic Analysis of a Swirl-Staged Turbulent Combustor," *AIAA Journal*, Vol. 44, No. 4, 2006, pp. 741–750. doi:10.2514/1.14689

[13] Smith, R., Nugent, N., Sisco, J., Xia, G., Anderson, W., Sankaran, V., and Merkle, C. L., "Experimental and Computational Investigation of Combustor Acoustics and Instabilities, Part I: Longitudinal Modes," 44th AIAA Aerospace Sciences Meeting and Exhibit, AIAA Paper 2006-0537, Reno, NV, Jan. 2006.

[14] Smith, R. J., "Computational Modeling of High Frequency Combustion Instability in a Single-Element Liquid Rocket Engine," M.S. Thesis, School of Aeronautics and Astronautics, Purdue Univ., West Lafayette, IN, Aug. 2006.

[15] Smith, R., Ellis, M., Xia, G., Sankaran, V., Anderson, W., and Merkle, C., "Computational Investigation of Acoustics and Instabilities in a Longitudinal-Mode Rocket Combustor," *AIAA Journal*, Vol. 46, No. 11, 2008, pp. 2659–2673. doi:10.2514/1.28125

[16] Ellis, M., Xia, G., Sankaran, V., and Merkle, C. L., "Acoustic Mode Simulations in Experimental Rocket Chambers," 41st AIAA/ASME/SAE/ASEE Joint Propulsion Conference, AIAA Paper 2005-4300, Tucson, AZ, July 2005.

[17] Habiballah, M., and Dubois, I., "Numerical Analysis of Engine Instability," *Liquid Rocket Engine Combustion Instability*, edited by V. Yang, and W. Anderson, Vol. 169, Progress in Astronautics and Aeronautics, AIAA, Washington, D.C., 1995, Chap. 18.

[18] Smith, R., Xia, G., Anderson, W., and Merkle, C. L., "Computational Modeling of Instabilities in a Single-Element Rocket Combustor Using a Response Function," 43rd AIAA/ASME/SAE/ASEE Joint Propulsion Conference, Cincinnati, OH, AIAA Paper 2007-5564, July 2007.

[19] Huang, Y., Wang, S., and Yang, V., "Systematic Analysis of Lean-premixed Swirl-Stabilized Combustion," *AIAA Journal*, Vol. 44, No. 4, 2006, pp. 724–740. doi:10.2514/1.15382

[20] Grenda, J. M., Sankaran, V., and Merkle, C. L., "Application of Computational Fluid Dynamics Techniques to Engine Instability Studies," *Liquid Rocket Engine Combustion Instability*, edited by V. Yang, and W. Anderson, Vol. 169, Progress in Astronautics and Aeronautics, AIAA, Washington, D.C., 1995, Chap. 19.

[21] Ducruix, S., Rey, C., and Candel, S., "A Method for the Transverse Modulation of Reactive Flows with Application to Combustion Instability," *Combustion Theory and Modeling*, Vol. 9, Feb. 2005, pp. 5–22. doi:10.1080/13647830500051950

[22] Tucker, P., Menon, S., Merkle, C., Oefelein, J., and Yang, V., "Validation of High-Fidelity CFD Simulations for Rocket Injector Design," 44th AIAA/ASME/ASEE Joint Propulsion Conference and Exhibit, Hartford CT, AIAA Paper 2008-5226, July 2008.

[23] Miller, K. J., "Experimental Study of Longitudinal Instabilities in a Single Element Rocket Combustor," M.S. Thesis, School of Aeronautics and Astronautics, Purdue Univ., West Lafayette, IN, May 2005.

[24] Miller, K. J., Nugent, N., Sisco, J., and Anderson, W., "Experimental Study of Combustion Instabilities in a Single-Element Coaxial Swirl Injector," 41st AIAA/ASME/SAE/ASEE Joint Propulsion Conference, Tucson, AZ, AIAA Paper 2005-4298, July 2005.

[25] Sisco, J. C., "Measurement and Analysis of an Unstable Model Rocket Combustor," Ph.D. Dissertation, Aeronautics and Astronautics Department, Purdue University, West Lafayette, IN, 2007.

[26] Yu, Y., Koeglmeier, S., Sisco, J. C., and Anderson, W. E., "Combustion Instability of Gaseous Fuels in a Continuously Variable Resonance Chamber (CVRC)," 44th AIAA/ASME/SAE Joint Propulsion Conference and Exhibit, Harford, CT, AIAA Paper 2008-4657, July 2008.

[27] Spalart, P. R., Jou, W.-H., Strelets, M., and Allmaras, S. R., "Comments on the Feasibility of LES for Wings, and on a Hybrid RANS/LES Approach," *1st AFOSR International Conference on DNS/LES*, Ruston, LA, Aug. 1997.

[28] Smith, D. A., and Zukoski, E. E., "Combustion Instability Sustained by Unsteady Vortex Combustion," 21st AIAA/ASME/SAE/ASEE Joint Propulsion Conference, Monterey, CA, AIAA Paper 1985-1248, June 1985.

[29] Li, D., Xia, G., Sankaran, V., and Merkle, C. L., "Computational Framework for Complex Fluids Applications," *3rd International Conference on Computational Fluid Dynamics*, Toronto, July 2004.

[30] Xia, G., Sankaran, V., Li, D., and Merkle, C. L., "Modeling of Turbulent Mixing Layer Dynamics in Ultra-High Pressure Flows," 36th AIAA Fluid Dynamics Conference and Exhibit, San Francisco, AIAA Paper 2006-3729, June 2006.

[31] Wilcox, D.C., *Turbulence Modeling for CFD*, 3rd ed., DCW Industries, Inc., La Cañada, CA, 2006.

[32] Menter, F. R., and Egorov, Y., "A Scale-Adaptive Simulation Model Using Two-Equation Models," AIAA Paper 2005-1095, 2005.

[33] Strutt, J. W., *The Theory of Sound*, Vol. 2, 2nd ed., Dover, New York, 1945.

[34] Chu, B. T., "Stability of Systems Containing a Heat Source—The Rayleigh Criterion," NACA RM 56D27, Washington, D.C., June 1956.

T. Jackson
Associate Editor